Advances in Materials Research, *Vol. 8, No. 3 (2019) 197-217*
DOI: https://doi.org/10.12989/amr.2019.8.3.197

Interfacial stresses in damaged RC beams strengthened by externally bonded prestressed GFRP laminate plate: Analytical and numerical study

Selma Chergui [1], Tahar Hassaine Daouadji [2], Mostefa Hamrat*[1], Bensaid Boulekbache [1], Abdelkader Bougara [1], Boussad Abbes [3] and Sofiane Amziane [4]

[1] *Hassiba Benbouali University of Chlef, Algeria*
[2] *Laboratory of Geomatics and sustainable development, University of Tiaret, Algeria*
[3] *GRESPI Laboratory, University of Reims, France*
[4] *Université Clermont Auvergne, Institut Pascal, Clermont-Ferrand, France*

(*Received July 18, 2019, Revised September 19, 2019, Accepted December 13, 2019*)

Abstract. In this study, the interfacial stresses in RC beams strengthened by externally bonded prestressed GFRP laminate are evaluated using an analytical approach, based on the equilibrium equations and boundary conditions. A comparison of the interfacial stresses obtained from the present analytical model and other existing models is undertaken. Otherwise, a parametric study is conducted to investigate the effects of geometrical and material properties on the variation of interfacial stresses in damaged RC beams strengthened by externally bonded prestressed GFRP laminate. The results obtained indicate that the damage degree has little effect on the maximum shear stress, with a variation less than 5% between the damaged and undamaged RC beams. However, the results also reveal that the prestressing level has a significant effect on the interfacial stresses; hence the damaged RC beam strengthened with an initial prestressing force of 100 kN gives 110% higher maximum shear stress than the damaged RC beam strengthened with an initial prestressing force of 50 kN. The values of shear stress obtained by the analytical approach are approximately equal to 44% of those obtained from the numerical solution, while the interfacial normal stresses predicted by the numerical study are approximately 26% higher than those calculated by the analytical solution.

Keywords: damaged beam; interfacial stresses; strengthening; prestressed GFRP laminate; analytical solution

1. Introduction

Strengthening of reinforced concrete (RC) structures is known to be useful to increase their service life. The service life of the RC structures may be reduced because of multiple pathologies (aging, defaults of shear strength or bending) due to excessive loadings, internal reinforcement corrosion, freeze-thaw action, poor initial design, etc. The rehabilitation and strengthening of structural members is oriented towards the use of composite materials (FRP materials), which are

*Corresponding author, Professor, E-mail: mhamrat@yahoo.fr

http://www.techno-press.org/?journal=amr&subpage=5 ISSN: 2234-0912 (Print), 2234-179X (Online)

able to improve their structural behavior efficiently (Meier 1995, Smith and Teng 2001, Tahar *et al*. 2019, Daouadji and Tounsi 2012, Rabia *et al*. 2019a, b, Hadj *et al*. 2019, Bensattalah 2018, Benhenni *et al*. 2018, Belkacem *et al*. 2018, Benhenni *et al*. 2019b, Abderezak *et al*. 2017, Bouakaz *et al*. 2014, Saribiyik and Caglar 2016). The common use of this strengthening technique for various structures (buildings, bridges…) has clearly demonstrated its efficiency and convenience (Meier 1995).

FRP materials include carbon fiber reinforced polymers (CFRP), glass fiber reinforced polymers (GFRP), aramid fiber reinforced polymers (AFRP) and combination of both of them. They were used over the past years in the form of sheets or laminates with an epoxy adhesive, to externally strengthen RC beams and slabs in flexure (shear strength) and confinement of circular columns (Attari *et al*. 2012). These FRP materials were found to avoid the need for demolition and replacement of construction. However, the problems of using FRP are its intolerance to uneven bonding surfaces (i.e., a high concentration of interface shear stress and normal peeling stress at the plate ends), which may cause peeling of the plate away from the concrete surface (substrate) and the possibility of brittle failure (Raithby 1982). In addition, the interfacial fracture between concrete and FRP initiated from an intermediate flexural or flexural-shear crack and critical diagonal crack, makes the problem more complex. As a result, the whole capacity of composite reinforcements could not be operated when using externally bonded reinforcement (EBR) technique due to debonding failure (Meier 2000, Wantanasiri and Lenwari 2015).

Numerous experimental studies have been conducted to mitigate the risk of premature debonding of FRP composite from concrete substrate (Hoque and Jumaat 2018). In these studies, the high local interface shear and peeling stresses at the ends of the FRP plates can be effectively countered by applying end anchorage systems i.e., the use of transverse sheets or straps, anchoring made from bi-directional fabric wrap and enhanced epoxy adhesion (Al-Mahaidi and Kalfat 2011).

Although all anchoring systems can improve bond performance, increase the ultimate loads up to 80% compared with conventional EBR strengthened specimen (Mostofinejad and Shameli 2013). However, the mechanism of premature failure has not yet been established due to numerous factors affecting the bond strength at the FRP-concrete interface.

Therefore, for further enhancement of the mechanical performance of the strengthened members, additional techniques should be developed. The prestressed CFRP strengthening method was used for strengthening or retrofitting RC structures. The advantages of such process can be summarized in increasing the load-carrying capacity and stiffness, creating a negative moment in the member and enhancing its properties (Aslam *et al*. 2015). This will enable the member to sustain higher loads and minimize the deflection and the optimal flexural stiffness; hence the risk of debonding is reduced (Oudah and El-Hacha 2013, Hoque and Jumaat 2018). The application of the prestressed CFRP strengthening method can also reduce the crack width and delay the onset of cracking, decrease the stress in the internal reinforcing steel and deflections and prevent the adhesive layer cracking (Aslam *et al*. 2015). Many researchers reported that prestressed FRPs plates represent an effective material for strengthening or retrofitting the damaged beams due to the combination of high interfacial shear and peeling (normal) stresses in the vicinity of the plate end (Li *et al*. 2018).

Thus, it is necessary to well understand the mechanism of the interfacial shear stresses between concrete and FRP sheets/laminates. In fact, the interfacial behavior between FRP and concrete is of critical importance in determining when failure occurs and how effectively the FRP is used in civil engineering applications. For the strengthening of the beams, local debonding initiates at an FRP plate end and at a location where high interfacial shear stresses arise from either the presence of a

defect as for instance a weak tensile strength of the concrete substrate or initiation of both flexural and shear cracking (Wu *et al*. 2018).

Many experimental (Zhou *et al*. 2017, Wu *et al*. 2018) analytical (Abderezak *et al*. 2018a, Smith and Teng 2001, Toutanji *et al*. 2013, Daouadji 2017 and 2013, Rabia *et al*. 2018, Bensattalah *et al*. 2019, Benhenni *et al*. 2019b, Abderezak *et al*. 2018b, Chedad *et al*. 2018, Daouadji *et al*. 2016) and numerical (Teng *et al*. 2002, Maalej and Leong 2005) works studied the interfacial shear stresses between concrete and FRP sheets. Maalej and Leong (2005) conclude from their investigation that interfacial stress increases with the increase of the number of CFRP layers. Smith and Teng (2001) and Teng *et al*. (2002) reported that the interfacial shear and normal stresses were constant across the thickness of the adhesive layer, although this result was not always right, because of the presence of different types of defects, such as bond defect, discontinuity in substrate (Zhou *et al*. 2017). However, the interfacial shear stresses reach their maximum value at the end of the adhesive layer (Toutanji *et al*. 2013, Wu *et al*. 2018).

Most of the previous research works focused on strengthening of undamaged RC beams with externally bonded sheets, whereas the interfacial stresses in damaged RC beams strengthened by externally bonded prestressed GFRP strips have not been fully studied yet.

In the present paper, the interfacial stresses in damaged RC beams strengthened with bonded prestressed GFRP composite plate are investigated using the analytical approach and the computational simulation. The simple approximate closed–form solutions applied in this paper provide a useful insight and simple tool for understanding the interfacial behavior of an externally bonded prestressed GFRP laminates on the damaged concrete beam. The analysis parameters include the prestressing force on adhesive stress, the laminate thickness, the adhesive layer thickness, the initial damage degree, the fiber orientation and the length of unstrengthened region.

2. Analytical approach

2.1 Assumptions of the solution

The following assumptions and simplifications were considered in this analytical study:

- All materials considered have linear-elastic behavior.
- A continuous adhesive bond between the RC beam and the composite plate.
- The bending moment in the composite plate (the adhesive) is neglected.
- The adhesive layer is assumed to be so thin that the interfacial shear and normal stresses are constant across the thickness of the adhesive.
- The bending stiffness of the composite plate is assumed to be negligible in comparison to that of the RC beam strengthened.
- No change in cross-section along the RC beam strengthened (i.e., no change for the plate, the beam or the adhesive dimensions).

2.2 Material properties of damaged plates

The model's Mazars is based on elasticity coupled with isotropic damage and ignores any manifestation of plasticity, as well as the closing of cracks (Mazars and Pijaudier-Cabot 1996). This concept directly describes the loss of rigidity and the softening behavior. The constraint is

determined by the following expression

$$\sigma_{ij} = (1-\phi)E_{ij}\varepsilon_{ij} \qquad 0 < \varphi < 1 \tag{1}$$

$$\tilde{E}_{11} = E_{11}(1-\phi)\ \text{long} \tag{2a}$$

$$\tilde{E}_{22} = E_{22}(1-\phi)\ \text{trans} \tag{2b}$$

where $\tilde{E}_{11}$, $\tilde{E}_{22}$ and E_{11}, E_{22} are the elastic constants of damaged and undamaged state, respectively. φ is damaged variable.

Hence, the material properties of the damaged plate can be represented by replacing the above elastic constants with the effective ones defined in Eqs. (2a) and (2b).

2.3 Basic equation of elasticity

Fig. 1 shows the strengthening of RC beam with a bonded prestressed GFRP laminate. From the equilibrium equation of forces in the horizontal direction of the RC beam depicted in Fig. 2, the axial force in RC beam $N_1(x)$ and GFRP laminate $N_2(x)$ are equal

$$N_1(x) = N_2(x) \tag{3}$$

The loss of prestressing force in the laminates is thus

$$\Delta P_L = P_0 - N_2 \tag{4}$$

where P_0 is the initial prestressing force in the laminate.

A differential segment of a plated beam is shown in Fig. 2, where the interfacial shear and normal stresses are denoted by τ(x) and σ(x), respectively. Fig. 2 also shows the positive sign convention for the bending moment, shear force, axial force and applied loading. Shear stress in the adhesive layer is directly related to the difference in deformation between the laminate and RC beam

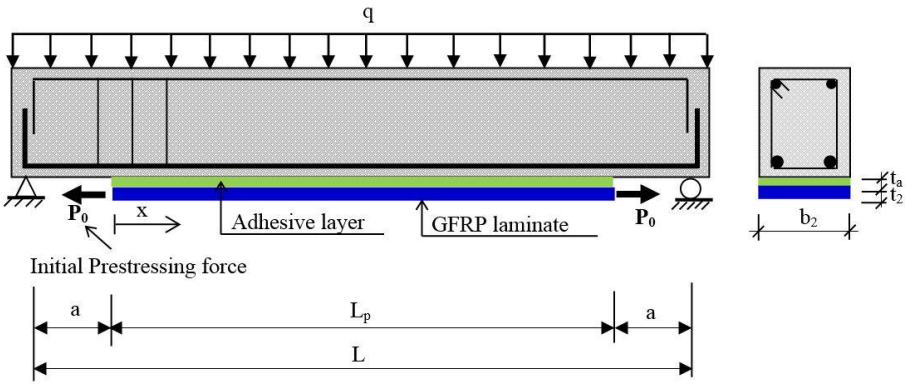

Fig. 1 Reinforced concrete beam strengthened by a prestressed bonded GFRP laminate

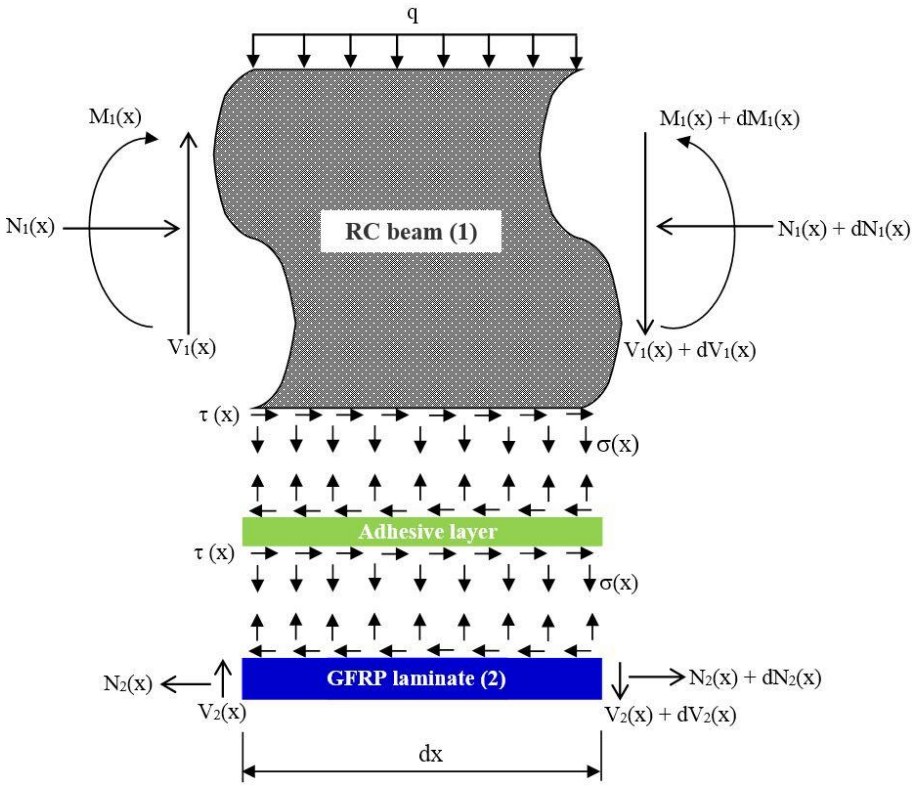

Fig. 2 Forces in differential element of the plated beam

$$\tau(x) = \frac{G_a}{t_a}[u_2(x) - u_1(x)] \tag{5}$$

where G_a, t_a, u_1 and u_2 denote the shear modulus, the thickness of the adhesive layer, the displacement of the RC beam and the displacement of the externally bonded prestressed laminate at the boundary of the bond, respectively.

Eq. (5) can be expressed in terms of the mechanical strain of the RC beam, $\varepsilon_1(x)$ and the prestressed laminate $\varepsilon_2(x)$ after differentiating the equation with respect to x.

$$\frac{d\tau(x)}{dx} = \frac{G_a}{t_a}[\varepsilon_2(x) - \varepsilon_1(x)] \tag{6}$$

$$\varepsilon_1(x) = \frac{du_1(x)}{dx}, \qquad \varepsilon_2(x) = \frac{du_2(x)}{dx} \tag{7}$$

Tensile strain at the bottom of the beam is induced by two basic stress components:

– Tensile stress induced by the bending moment $M_1(x)$ in the beam,
– Axial stress induced by the adhesive shear stress at the bond interface.

Therefore, Eq. (7) can be written as follows

$$\varepsilon_1(x) = \frac{du_1(x)}{dx} = \frac{y_1}{\tilde{E}_{11} I_1} M_1(x) + \frac{N_1}{\tilde{E}_{11} A_1} \tag{8}$$

where A_1, I_1 and $\tilde{E}_{11}$are the cross-sectional area, the second moment of area and the modulus of elasticity of the RC beam respectively.

The change in axial strain in the laminate due to the deformability of the RC beam can be related to the loss in the prestressing force as follows

$$\varepsilon_2(x) = \frac{du_2(x)}{dx} = A'_{11} \frac{(N_2(x) + P_0)}{b_2} - D'_{11} \frac{y_2}{b_2} M_2(x) + \frac{t_2}{3G_2} \frac{d\tau_a}{dx} \tag{9}$$

where t_2 and b_2 represent the thickness and the width of the GFRP laminate, respectively.

Since the composite laminate is an orthotropic material, its material properties vary from layer to layer. In the current study, laminate theory is used to determine the stress and strain behaviors of an externally bonded composite plate in order to investigate the whole mechanical performance of the composite-strengthened structures. The effective modulus of the composite laminate is varied by the orientation of fiber directions and arrangements of the laminate patterns.

Eq. (9) is only valid for the plate for which the mechanical properties behave isotropically and homogeneously. Therefore, laminate theory is used to estimate the strain of the composite plate (Shen *et al*. 2004)

$$\begin{Bmatrix} \varepsilon_0 \\ k \end{Bmatrix} = \begin{bmatrix} A^x & B^x \\ B^x & D^x \end{bmatrix} \begin{Bmatrix} N \\ M \end{Bmatrix} = \begin{bmatrix} A & B \\ B & D \end{bmatrix}^{-1} \begin{Bmatrix} N \\ M \end{Bmatrix} \tag{10}$$

where ε_0 and k are in-plane strain and bending curvature vectors of the laminated plate. N and M are the in-plane resultants and the bending moments, respectively. Stiffness components of the laminate are given as follows

– Extensional matrix

$$A_{ij} = \sum_{kl=1}^{NL} \left(\overline{Q_{ij}}\right)_{kl} (z_{kl} - z_{kl-1}) \tag{11a}$$

– Extensional-bending coupled matrix

$$B_{ij} = \frac{1}{2} \sum_{kl=1}^{NL} \left(\overline{Q_{ij}}\right)_{kl} (z_{kl}^2 - z_{kl-1}^2) \tag{11b}$$

– Flexural matrix

$$D_{ij} = \frac{1}{3} \sum_{kl=1}^{NL} \left(\overline{Q_{ij}}\right)_{kl} (z_{kl}^3 - z_{kl-1}^3) \tag{11c}$$

where the subscript NL represents the number of laminate layers of the FRP plate. $\left(\overline{Q_{ij}}\right)_{kl}$ are the transformed stiffness's of the layer number "k_l" of the laminate and can be estimated by using the off-axis orthotropic ply theory (Shen *et al*. 2004).

A schematic diagram illustrating the laminate theory for a composite plate is shown in Fig. 3. Assume that the ply arrangement of the plate is symmetrical with respect to the mid-plane axis Z = 0. Significant simplification in laminate analysis then occurs by assuming that the coupling matrix B is identically zero (Roberts 1989).

Furthermore, it is assumed that no external bending moment is applied to the plate. Therefore Eq. (7) can be simplified to the following matrix form for a laminate with a width b_2

$$\{\varepsilon_0\} = [A^x]\{N\}_2 \tag{12}$$

$$\{\varepsilon_0\} = \begin{Bmatrix} \varepsilon_x \\ \varepsilon_y \\ \varepsilon_{xy} \end{Bmatrix} \quad \text{and} \quad \{N\}_2 = \begin{Bmatrix} N_x \\ N_y \\ N_{xy} \end{Bmatrix} \tag{13}$$

In the present study, only an axial load in the beam's longitudinal axis is considered, i.e., $N_y = N_{xy} = 0$. Therefore, Eq. (12) can be simplified to

$$\varepsilon_2(x) = A_{11}^X N_x \frac{1}{b_2}; \qquad N_x = P_0 - N_2(x) \tag{14}$$

It is well known in many studies, that the material properties of composite are function of temperature and moisture (Tounsi and Amara 2005). In terms of a micromechanical model of laminate, the materials properties may be written as

$$E_L = V_f E_f + V_m E_m \tag{15}$$

$$\frac{1}{E_T} = \frac{V_f}{E_f} + \frac{V_m}{E_m} - V_f V_m \frac{\nu_f^2(\frac{E_m}{E_f}) + \nu_m^2(\frac{E_f}{E_m}) - 2\nu_f\nu_m}{V_f E_f + V_m E_m} \tag{16}$$

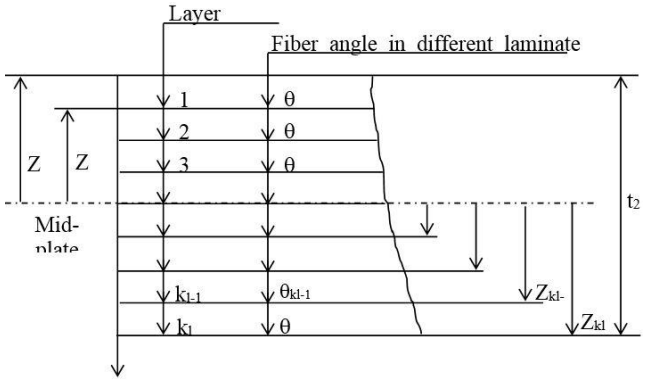

Fig. 3 Multi-layered laminate geometry

$$\frac{1}{G_{LT}} = \frac{V_f}{G_f} + \frac{V_m}{G_m} \tag{17}$$

$$\nu_{LT} = V_f \nu_f + V_m \nu_m \tag{18}$$

E_f, G_f and ν_f are the Young's modulus, shear modulus and Poisson's ratio, respectively, of the GFRP laminate, and E_m, G_m and ν_m are the corresponding properties for the matrix.

In the above equation, V_f and V_m are fiber and matrix volume fractions and are related by

$$V_f + V_m = 1 \tag{19}$$

2.3.1 Shear stress distribution along the FRP–concrete interface

The governing differential equation for the interfacial shear stress is expressed as follows (Hassaine Daouadji *et al*. 2008)

$$\begin{aligned} &\frac{d^2\tau(x)}{dx^2} - K_1\left(A_{11}^{'} + \frac{b_2}{\tilde{E}_{11}A_1} + \frac{(y_1+y_2)(y_1+y_2+t_a)}{\tilde{E}_{11}I_1D_{11}^{'} + b_2} b_2 D_{11}^{'}\right)\tau(x) \\ &+K_1\left(\frac{(y_1+y_2)}{\tilde{E}_{11}I_1D_{11}^{'} + b_2} D_{11}^{'}\right)V_T(x) = 0 \end{aligned} \tag{20a}$$

$$K_1 = \frac{1}{\left(\frac{t_a}{G_a} + \frac{t_2}{3G_2}\right)} \tag{20b}$$

For simplicity, the general solutions presented below are limited to loading which is either concentrated or uniformly distributed over part or the whole span of the beam, or both. For such loading, $d^2V_T(x)/dx^2 = 0$, and the general solution of Eq. (20a) is given by

$$\tau(x) = B_1 \cos h\,(\lambda x) + B_2 \sin h\,(\lambda x) + m_1 V_T(x) \tag{21}$$

where

$$\lambda^2 = K_1\left(A_{11}^{'} + \frac{b_2}{\tilde{E}_{11}A_1} + \frac{(y_1 + t_2/2)(y_1 + t_a + t_2/2)}{\tilde{E}_{11}I_1D_{11}^{'} + b_2} b_2 D_{11}^{'}\right) \tag{22}$$

$$m_1 = \frac{K_1}{\lambda^2}\left(\frac{(y_1 + t_2/2)}{\tilde{E}_{11}I_1D_{11}^{'} + b_2} D_{11}^{'}\right) \tag{23}$$

B_1 and B_2 are constant coefficients determined from the boundary conditions. In the present study, a simply supported beam was investigated which is subjected uniformly distributed load. The interfacial shear stress for this load case at any point is written as follows (Hassaine Daouadji *et al*. 2008)

$$\tau(x) = B_1 \cos h\,(\lambda x) + B_2 \sin h\,(\lambda x) + m_1 q\left(\frac{L}{2} - x - a\right) \qquad 0 \le x \le L_p \tag{24}$$

where q is the uniformly distributed load, x, a, L and L_p are defined in Fig. 1.

The constants of integration need to be determined by applying suitable boundary conditions:

(1) Owing to symmetry, all displacements at the middle of the composite beam are zero.

$$u_2(x = L_p/2) = u_1(x = L_p/2) = 0 \tag{25}$$

Which, substituted in Eq. (5), $\tau(x = L_p/2) = 0$ and together with Eq. (24)

$$B_1 = -B_2 \tan h\left(\lambda \frac{L_p}{2}\right) \tag{26}$$

For practical cases $\lambda L_p/2 > 10$and as a result$tan\, h\left(\lambda L_p/2\right) \approx 1$, so the expression of B_1 can be simplified to $B_1 = -B_2$.

(2) At the end of the laminate:

$$N_2(x = 0) = N_1(x = 0) = 0 \quad \text{and} \quad M_1(x = 0) = \frac{qa}{2}(L - a) \tag{27}$$

Inserting in Eq. (6) gives

$$\frac{d\tau(x = 0)}{dx} = \frac{G_a}{t_a}\left[\frac{A_{11}^*}{b_2}P_0 - \frac{ha}{4\tilde{E}_{11}I_1}q(L - a)\right] \tag{28}$$

By substituting Eq. (24) into Eq. (28), B_2 can be determined as follows

$$B_2 = \frac{G_a}{\lambda t_a}\left[\frac{A_{11}^*}{b_2}P_0 - \frac{ha}{4\tilde{E}_{11}I_1}q(L - a)\right] + \frac{m_1}{\lambda}q \tag{29}$$

Substitution of B_1 and B_2 into Eq. (24) gives an expression for interfacial shear stress at any point

$$\tau(x) = -B_2 e^{-\lambda x} + m_1 q\left(\frac{L}{2} - x - a\right) \tag{30}$$

The distribution of the axial force in the laminate can be found by deriving Eq. (30) once and substituting the left-hand side in Eq. (6)

$$\lambda B_2 e^{-\lambda x} - m_1 q = \frac{G_a}{t_a}\left(\frac{A_{11}^x}{b_2}P_0 - \frac{A_{11}^x}{b_2}P_2(x) - \frac{M_1(x)}{I_1\tilde{E}_{11}}\frac{h}{2} + \frac{P_1(x)}{A_1\tilde{E}_{11}}\right) \tag{31}$$

Using the following Eqs. (32) and (33) we obtain Eq. (34)

$$N_2(x) = N_1(x) \tag{32}$$

$$M_1(x) = \frac{qa}{2}(x + a) - \frac{qa}{2}(x + a)^2 + P_2(x)\frac{h}{2} \tag{33}$$

$$N_2(x) = \frac{b_2 G_a}{\lambda^2 t_a}\left[\frac{A_{11}^x}{b_2}P_0(1-e^{-\lambda x}) - q\begin{pmatrix} \frac{Lh}{4\tilde{E}_{11}I_1}(x+a) - \frac{h}{4\tilde{E}_{11}I_1}(x+a)^2 \\ -\frac{ha}{4\tilde{E}_{11}I_1}(L-a)e^{-\lambda x} - \frac{t_a}{G_a}m_1(1-e^{-\lambda x}) \end{pmatrix}\right] \quad (34)$$

2.3.2 Normal stress distribution along the FRP–concrete interface

The following governing differential equation for the interfacial normal stress (Hassaine Daouadji *et al*. 2008)

$$\frac{d^4\sigma_n(x)}{dx^4} + K_n\left(D_{11}^{'} + \frac{b_2}{\tilde{E}_{11}I_1}\right)\sigma_n(x) - K_n\left(D_{11}^{'}\frac{t_2}{2} - \frac{y_1 b_2}{\tilde{E}_{11}I_1}\right)\frac{d\tau(x)}{dx} + \frac{qK_n}{\tilde{E}_{11}I_1} = 0 \quad (35)$$

The general solution to this fourth–order differential equation is

$$\begin{aligned}\sigma_n(x) = {} & e^{-\beta x}[C_1\, cos(\beta x) + C_2\, sin(\beta x)] \\ & + e^{\beta x}[C_3\, cos(\beta x) + C_4\, sin(\beta x)] - n_1\frac{d\tau(x)}{dx} - n_2 q\end{aligned} \quad (36)$$

For large values of x it is assumed that the normal stress approaches zero and, as a result, $C_3 = C_4 = 0$. The general solution therefore becomes

$$\sigma_n(x) = e^{-\beta x}[C_1\, cos(\beta x) + C_2\, sin(\beta x)] - n_1\frac{d\tau(x)}{dx} - n_2 q \quad (37)$$

where

$$\beta = \sqrt[4]{\frac{K_n}{4}\left(D_{11}^{'} + \frac{b_2}{\tilde{E}_{11}I_1}\right)} \quad (38)$$

$$n_1 = \left(\frac{y_1 b_2 - D_{11}^{'}\tilde{E}_{11}I_1 t_2/2}{D_{11}^{'}\tilde{E}_{11}I_1 + b_2}\right) \quad (39)$$

$$n_2 = \frac{1}{D_{11}^{'}\tilde{E}_{11}I_1 + b_2} \quad (40)$$

The above expressions for the constants C_1 and C_2 has been left in terms of the bending moment $M_T(0)$ and shear force $V_T(0)$ at the end of the soffit plate. The constants C_1 and C_2 are determined by considering appropriate boundary conditions. The first boundary condition is the zero bending moment at the ends of the soffit plate. The resulting expression yields the following relationship at the plate end, by differentiating Eq. (37)

$$\frac{d^2\sigma(x=0)}{dx^2} = \frac{E_a}{t_a}\left[\frac{1}{\tilde{E}_{11}I_1}M_1(0) - \frac{D_{11}^*}{b_2}M_2(0)\right] \quad (41)$$

However, the moment at the plate end $M_2(0)$ is zero. As a result, the above relationship can be expressed as follows

$$\frac{d^2\sigma(x=0)}{dx^2} = \frac{E_a}{t_a\tilde{E}_{11}I_1}M_1(0) \tag{42}$$

Boundary condition 2 concerns the shear force at the end of the soffit plate in the beam and the soffit plate. The resulting expression yields the following relationship at the plate end, by differentiating Eq. (37)

$$\frac{d^3\sigma(x=0)}{dx^3} = \frac{E_a}{t_a}\left[\frac{1}{\tilde{E}_{11}I_1}V_1(0) - \frac{D_{11}^*}{b_2}V_2(0)\right] - \frac{E_a}{t_a}\left(\frac{b_2h}{2\tilde{E}_{11}I_1} - \frac{t_2}{2}D_{11}^*\right)\tau(0) \tag{43}$$

As the applied shear force at the end of the plate is zero (i.e., $V_2(0) = 0$). The second boundary condition can therefore be expressed as

$$\frac{d^3\sigma(x=0)}{dx^3} = \frac{E_a}{t_a\tilde{E}_{11}I_1}V_1(0) - n_3\tau(0) \tag{44}$$

$$n_3 = \frac{E_a}{t_a}\left(\frac{b_2h}{2\tilde{E}_{11}I_1} - \frac{t_2}{2}D_{11}^*\right) \tag{45}$$

Further differentiation of Eq. (37) leads to the following expressions for the second and third derivatives of the interfacial normal stress at the plate end.

$$\frac{d^2\sigma(x=0)}{dx^2} = -\beta^2C_2 - n_1\frac{d^3\tau(x=0)}{dx^3} - n_2\frac{d^2q}{dx^2} \tag{46}$$

$$\frac{d^3\sigma(x=0)}{dx^3} = 2\beta^3C_1 + 2\beta^2C_2 - n_1\frac{d^4\tau(x=0)}{dx^4} - n_2\frac{d^3q}{dx^3} \tag{47}$$

Since the loading is limited to either uniformly distributed or concentrated loads, the second and higher order derivatives of q become zero. Substituting the boundary conditions into the above two equations leads to the determination of C_1 and C_2 as follows

$$C_1 = \frac{E_a}{2\beta^3t_a\tilde{E}_{11}I_1}[V_1(0) + \beta M_1(0)] - \frac{n_3}{2\beta^3}\tau(0) + \frac{n_1}{2\beta^3}\left(\frac{d^4\tau(x=0)}{dx^4} + \beta\frac{d^3\tau(x=0)}{dx^3}\right) \tag{48}$$

$$C_2 = -\frac{E_a}{2\beta^2t_a\tilde{E}_{11}I_1}M_1(0) - \frac{n_1}{2\beta^2}\frac{d^3\tau(x=0)}{dx^3} \tag{49}$$

3. Comparison between numerical and analytical interfacial stresses

The modeling process using Abaqus model (ABAQUS 2007) defines the different components of the model separately, notably the reinforced concrete beam, the GFRP laminate and the adhesive layer, each one compatible with the other in order to perform a complete analysis. We

know that the modeling is an iterative process; it will take a number of analyses enabling to simulate successfully a particular set of characteristics. A 4-node linear quadrilateral, type S4R was performed, in which half of the beam was considered because of the symmetric geometry and loading of the beam. All the nodes at mid-span were limited to make the needed symmetry, and the nodes at the end of the RC beam were restrained to reflect the conditions of a simply roll-supported. The number of elements used is related to the geometric parameters such as the length and the cross-sectional perimeter. Accurate stress results are expected at the ends of the plate when a fine mesh is deployed in these areas.

A comparison of the interfacial shear and normal stresses from the present analytical model reviewed earlier with those of Smith (Smith and Teng 2001), Tounsi (Tounsi *et al*. 2009) and Hassaine Daouadji (Hassaine Daouadji *et al*. 2016) is made for undamaged RC beams strengthened by externally bonded without prestressing force ($P_0 = 0$ and $\varphi = 0$). The beam is simply supported and subjected to uniformly distributed load (q = 50 kN/m). The relevant geometrical and mechanical properties of the composite beam used in the finite element analysis were the same as those used in the analytical method of the RC beams; the adhesive layer and the GFRP laminate are given in Table 1.

The results of the peak interfacial shear and normal stresses for RC undamaged beams with bonded non-prestressed GFRP laminates are shown in Table 2. From these results, it can be seen that the present analytical solution agrees closely with the solutions of Tounsi (Tounsi *et al*. 2009) and Hassaine Daouadji (Hassaine Daouadji *et al*. 2016), except for that of Smith and Teng' solution (Smith and Teng 2001), where values are slightly higher for both normal and shear stresses. In addition, the results of the present analytical solution differ from those of the numerical results by about 16% for shear stress, with the analytical values of shear stress being higher (Table 2).

Table 1 Geometric and material properties of the composite beam

Component	Width (mm)	Depth (mm)	Length (mm)	E11 (GPa)	E22 (GPa)	G12 (GPa)	ν
RC beam	200	300	2800	30	30	-	0.18
Adhesive layer	200	2	variable	3	3	-	0.35
GFRP laminate	200	4	variable	50	10	5	0.28

Table 2 Comparison of peak interfacial stresses for RC undamaged beams with bonded non-prestressed GFRP laminates

Load	Theory	Shear stress (MPa)	Normal stress (MPa)
Uniformly distributed load	Present solution - Analytical model	1.5887	1.1079
	Present solution - Numerical model - MEF	1.3753	1.3481
	Hassaine Daouadji - Analytical model (2016)	1.5923	1.1101
	Hassaine Daouadji - Numerical model (2016)	1.3789	1.3503
	Tounsi - Analytical model (2009)	1.6142	1.1133
	Smith and Teng - Analytical model (2001)	1.6931	1.1678

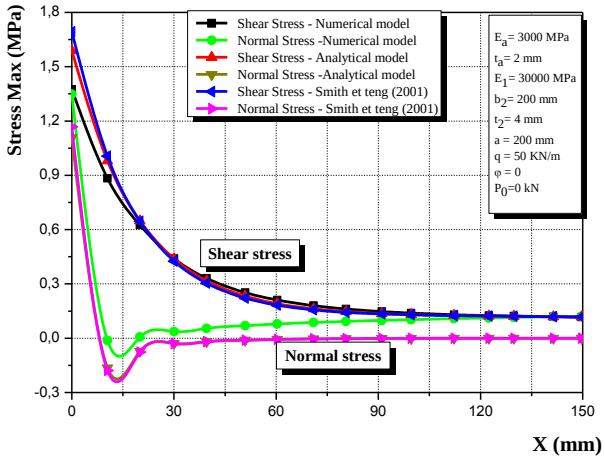

Fig. 4 Variations of interfacial stresses in RC beam bonded with GFRP laminate: Comparison between the analytical and numerical values

The analytical results for the interfacial stresses obtained from the present analytical solution shown in Fig. 4, are compared with that of Smith and Teng's solution (Smith and Teng 2001). Overally, there is a reasonably close agreement between the numerical and the analytical results, with small differences only in a tiny zone at the plate end. However, the analytical interfacial normal stress values are different with the finite element values, which are higher.

4. Parametric study

To validate the present analytical solution, the interfacial stresses are calculated and compared with the numerical results, taking into account the effect of some parameters on the distributions of the normal and shear stresses in a damaged RC beams strengthened by externally bonded with prestressed GFRP laminate.

4.1 Effect of the prestressing force on adhesive stresses

In this section, a comparison is made between the results of the shear stresses of the present analytical model and those of the numerical model, for RC beam damaged at the level $\varphi = 0.3$ and strengthened with bonded prestressed GFRP laminate at different prestressing force P_0 (P_0 = 0, 50 and 100 kN). The interfacial shear and normal stresses distributions for the damaged RC beam strengthened with bonded prestressed GFRP laminate are shown in Figs. 5 and 6.

The results in Figs. 5 and 6 indicate that the values of interfacial stresses at the end of the prestressed laminate increase when the prestressing force increases. Indeed, the damaged RC beam strengthened with an initial prestressing force of 100 kN has a maximum shear stress 110% higher than that of the damaged RC beam strengthened with an initial prestressing force of 50 kN. This is because of the increase of the value of the prestressing force P_0, which has lead to high stress concentrations.

Otherwise, significant differences are found between numerical and analytical models results at the end of the GFRP laminate, particularly for the interfacial shear stress. The highest value for the

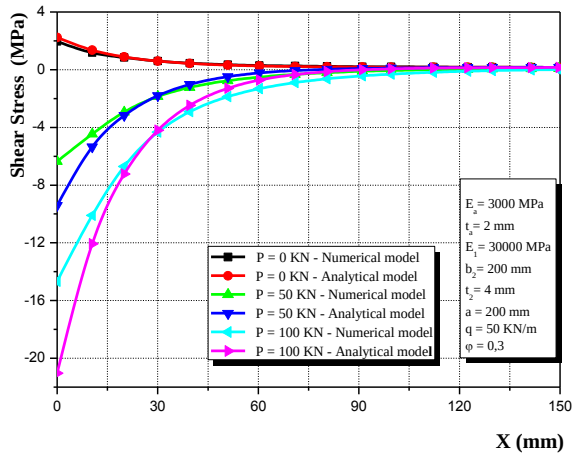

Fig. 5 Adhesive shear stress in a damaged RC beam strengthened with bonded prestressed GFRP laminate

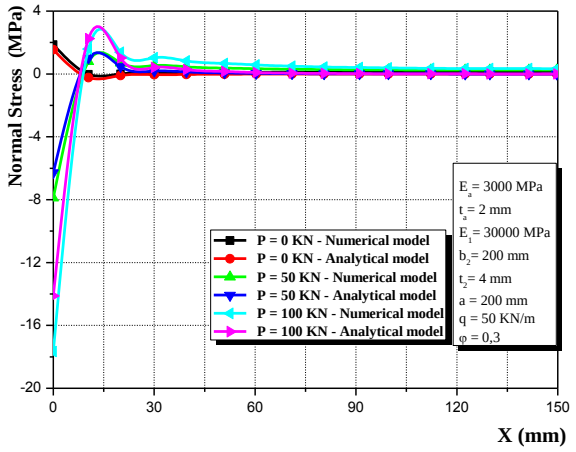

Fig. 6 Variations of Adhesive normal stress along the x direction in a damaged RC beam with different prestressing force P_0

peak interfacial shear stress, which is determined by analytical model, is 1.45 times lower than that provided by the numerical model. However, for the interfacial normal stress, the largest value, computed by the numerical solution is 1.30 times lower than that given by the analytical solution. In addition, a good agreement is found between numerical and analytical models for both interfacial stresses, beyond at 20 mm from the end of the plate (Figs. 5 and 6).

4.2 Effect of the laminate thickness

For an initial prestressing force kept constant (P = 100 kN) and at different degrees of damage, the effect of the thickness of the GFRP laminate on the interfacial stresses at the end of a prestressed laminate is presented in Table 3, where t_2 denotes the thickness of the GFRP laminate.

From Table 3, it can be seen that the normal and shear stresses decrease when the plate

Table 3 Effect of the laminate thickness on edge stresses in damaged RC beam bonded prestressed GFRP laminate

	x = 0 P_0 = 100 kN							
Damage degree	t_2 = 2 mm		t_2 = 4 mm		t_2 = 6 mm		t_2 = 8 mm	
	Shear stress (MPa)	Normal stress (MPa)	Shear stress (MPa)	Normal stress (MPa)	Shear stress (MPa)	Normal stress (MPa)	Shear stress (MPa)	Normal stress (MPa)
φ = 0	-34.202	-19.843	-22.081	-14.888	-16.459	-12.077	-13.008	-10.105
φ = 0.1	-33.992	-19.715	-21.805	-14.687	-16.144	-11.824	-12.667	-9.812
φ = 0.2	-33.732	-19.555	-21.463	-14.440	-15.756	-11.514	-12.251	-9.455
φ = 0.3	-33.401	-19.351	-21.032	-14.127	-15.269	-11.125	-11.731	-9.010

thickness increases. This is attributed to the decrease of the level of stress concentration as the increase of the GFRP laminate thickness. Also, it can be noted that the interfacial shear stress is higher than the interfacial normal stress, about 73.3% difference was observed between these stresses at t_2 = 2 mm regardless the level of damage. Moreover, the interfacial stresses at the end of the prestressed plate of damaged RC beams were found to be significantly lower than those of the undamaged ones; the maximum difference reaches 11% when t_2 = 8 mm, φ = 0 and φ = 0.3 for both interfacial stresses.

4.3 Effect of adhesive layer thickness

The thickness of the adhesive layer is an important parameter, where both the shear and normal stresses vary considerably in the close vicinity of the end of the adhesive layer. Table 4 shows the effect of varying the adhesive layer thickness on the interfacial stresses for damaged RC beams as a function of the damage degrees (φ).

According to Table 4, the values of the interfacial stresses at the end of the laminate decrease with the increase of the adhesive thickness (from 1 to 4 mm). It can be seen also that reducing the thickness of the adhesive layer leads to the enhancement of the shear stress, despite its effect on the transverse normal stress is less significant. It is noted that the difference in interfacial stresses between the damaged (φ = 0.3) and undamaged (φ = 0) RC beams is not significant, with

Table 4 Effect of varying the thickness of adhesive layer on interfacial stresses at the ends of bonded prestressed GFRP laminate (X = 0, P_0 = 100 kN)

	x = 0 P_0 = 100 kN					
Damage degree	t_2 = 1 mm		t_2 = 2 mm		t_2 = 4 mm	
	Shear stress (MPa)	Normal stress (MPa)	Shear stress (MPa)	Normal stress (MPa)	Shear stress (MPa)	Normal stress (MPa)
φ = 0	-29.437	-23.212	-22.081	-14.888	-16.102	-9.296
φ = 0.1	-29.074	-22.903	-21.805	-14.687	-15.896	-9.169
φ = 0.2	-28.626	-22.521	-21.463	-14.440	-15.642	-9.012
φ = 0.3	-28.059	-22.039	-21.032	-14.127	-15.320	-8.813

a variation not more than 5%, for any adhesive layer thickness used.

4.4 Effect of the initial damage degree on the maximal interfacial stresses

Table 5 illustrates the effect of the different initial damage degrees on the maximum shear and the normal interfacial stresses in RC beam strengthened with bonded prestressed GFRP laminate. It also shows the comparison between the analytical and numerical results for interfacial stresses.

According to Table 5, it can be observed that both shear and normal stresses decrease slightly with the increase of the initial damage degree (from $\varphi = 0$ to 0.3). So, it should be mentioned that these interfacial stresses are very small at x = 50 mm and 100 mm from the GFRP laminate end. In the same context, the results provided in Table 5 indicate that the analytical values of the shear stresses are approximately 44% higher than those obtained from the numerical analysis, while the interfacial normal stresses predicted by the numerical results are approximately 26% higher than those calculated by the analytical solution.

4.5 Effect of fiber orientation

Fiber orientation is an important variable in the structural design of FRP wrapped RC beams. In fact, the structural capacity of FRP can be tailored and maximized by aligning fibers along the optimal orientation.

For the section studied, various fiber orientations were used, notably 0°, 15°, 30°, 45°, 60°, 75° and 90° from the axial (loading) direction. The interfacial stresses for damaged RC beam plotted as function of the fiber orientation are shown in Fig. 7. It can be seen that when fibers are aligned in beam's longitudinal direction x (0°), it leads to the lowest values of the interfacial stresses,

Table 5 Effect of initial damage degree on the maximal interfacial stresses at different distances from the laminate end

Damage degree	Numerical	Analytical	Numerical	Analytical
	Shear stress (MPa)		Normal stress (MPa)	
	x = 0 P = 100 kN			
$\varphi = 0$	-15.359	-22.081	-18.787	-14.888
$\varphi = 0.1$	-15.186	-21.805	-18.490	-14.687
$\varphi = 0.3$	-14.672	-21.032	-17.662	-14.127
	X = 50 mm P = 100 kN			
	Shear stress (MPa)		Normal stress (MPa)	
$\varphi = 0$	-1.996	-1.476	0.566	0.166
$\varphi = 0.1$	-1.965	-1.425	0.594	0.163
$\varphi = 0.3$	-1.873	-1.286	0.665	0.154
	X = 100 mm P = 100 kN			
	Shear stress (MPa)		Normal stress (MPa)	
$\varphi = 0$	-0.308	-0.007	0.292	0.013
$\varphi = 0.1$	-0.310	0.010	0.317	0.013
$\varphi = 0.3$	-0.309	0.056	0.384	0.012

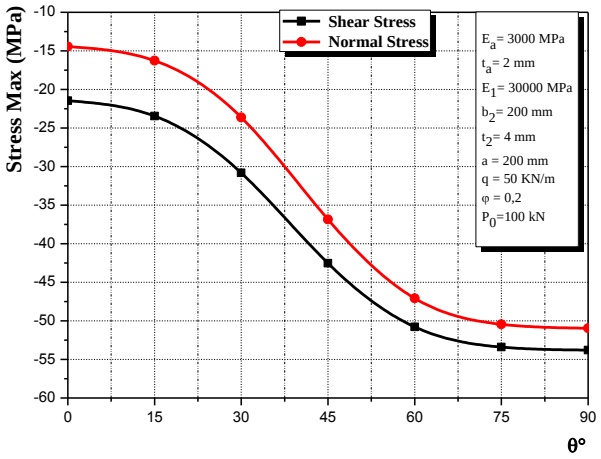

Fig. 7 Effect of various fiber orientations on interfacial stresses for damaged RC beam (φ = 0.2)

while the fibers are oriented at 90°, the interfacial shear and normal stresses reach the highest values. This is because when fibers are oriented in the beam direction (0°), it provides the highest E-modulus of the plate, which leads to the reduction of the interfacial stresses intensity, as shown in Fig. 7. Moreover, the shear stress is higher than the transverse normal stress, for fiber with 0° orientation. This difference was found to be relatively small for fibers oriented at 90° from the loading direction.

4.6 Effect of the length of unstrengthened region

Table 6 gives the results of the influence of the length of unstrengthened region "a" on the interfacial stresses, where "a" indicates the length between the end of the composite laminate and the beam support. It is clear from Table 6 that, the plate terminates further away from the supports, as the interfacial stresses decrease significantly. Thereby, the interfacial stresses of the beam with 50 mm length, was larger than those of the beam with 300 mm length, as the GFRP bonded length of the former was longer than that of the latter. It is noteworthy that the longer bonded length of

Table 6 Effect of the length of the unstrengthened region "a" on the interfacial stress at the ends of bonded prestressed GFRP laminate

	x = 0 P_0 = 100 kN							
Damage degree	a = 50 mm		a = 100 mm		a =200 mm		a = 300 mm	
	Shear stress (MPa)	Normal stress (MPa)	Shear stress (MPa)	Normal stress (MPa)	Shear stress (MPa)	Normal stress (MPa)	Shear stress (MPa)	Normal stress (MPa)
φ = 0	-23.139	-15.617	-22.773	-15.365	-22.081	-14.888	-21.440	-14.447
φ = 0.1	-22.975	-15.493	-22.571	-15.214	-21.805	-14.687	-21.096	-14.200
φ = 0.2	-22.773	-15.341	-22.321	-15.029	-21.463	-14.440	-20.671	-13.895
φ = 0.3	-22.518	-15.148	-22.004	-14.795	-21.032	-14.127	-20.132	-13.509

the GFRP plate leads to the more ductile failure (Attari *et al*. 2012).

For the beam with the shorter GFRP length (a = 300 mm), the interfacial shear stress distributions were mainly localized within the two end zones of the bondline. Thus, the debonding failure occurred more easily because of the lack of anchorage length (i.e., short bond length of GFRP laminate).

Another interesting observation to be mentioned is when a long GFRP plate (a = 50 mm) is used, the interfacial shear stresses are more highly and uniformly distributed along the bondline; thus the magnitude of the interfacial normal stresses are lowered. Therefore, it is recommended to extend as much as possible the strengthening strip to the bondlines.

5. Conclusions

The study of the interfacial stresses at both ends of the bondline has a significant role in understanding the premature brittle failure of RC beams strengthened with bonded prestressed GFRP laminate and has lead to the following conclusions:

(1) For the case of undamaged RC beams strengthened by externally bonded without prestressing force, the suggested analytical solution agrees closely with the solutions of Tounsi (Tounsi *et al*. 2009) and Hassaine Daouadji (Hassaine Daouadji *et al*. 2016), except for Smith and Teng's solution, where values are slightly higher for both normal and shear stresses. However, the results of the shear stress deduced from the analytical solution are 16% higher than those resulted from the numerical study.
(2) The damage degree has a little effect on the maximum shear stress, with a variation not more than 5% between the damaged and undamaged RC beams. In addition, the values of shear stress at the end of the prestressed laminate found by the analytical study are approximately 44% higher than those obtained from the numerical analysis, while the interfacial normal stresses predicted by the numerical method are approximately 26% higher than those calculated by the analytical solution.
(3) The damaged RC beam strengthened with an initial prestressing force of 100 kN presents a maximum shear stress 110% higher than that strengthened with an initial prestressing force of 50 kN. Otherwise, the highest value for the peak interfacial shear stress, given by the analytical model is 1.45 times lower than that resulted from the numerical model. However, a good agreement is observed between these two models for both interfacial stresses, beyond 20 mm from the end of the GFRP laminate.
(4) The increase in both GFRP laminate and adhesive layer thickness leads to the decrease of the interfacial stresses. In other words, the interfacial shear stress is higher than that of the normal stress with a difference of 73.3%.
(5) The shear stress is found to be higher than that of the transverse normal for fiber with 0° orientation; however this difference is relatively small when fibers are oriented at 90° from the loading direction.
(6) As the plate terminates further away from the supports, the interfacial stresses decrease significantly. Furthermore, the interfacial shear stresses were more highly and uniformly distributed along the bondline. While, the magnitude of the interfacial normal stresses was lowered particularly for the longer bonded length of the GFRP laminate (a = 50 mm).

References

ABAQUS (2007), User's Manual, Version 6.7.0, Hibbitt, Karlsson & Sorensen, Inc. Pawtucket, RI, USA.

Abderezak, R., Daouadji, T.H., Abbes, B., Rabia, B., Belkacem, A. and Abbes, F. (2017), "Elastic analysis of interfacial stress concentrations in CFRP-RC hybrid beams: Effect of creep and shrinkage", *Adv. Mater. Res., Int. J.*, **6**(3), 257-278. https://doi.org/10.12989/amr.2017.6.3.257

Abderezak, R., Rabia, B., Daouadji, T.H., Abbes, B., Belkacem, A. and Abbes, F. (2018a), "Elastic analysis of interfacial stresses in prestressed PFGM-RC hybrid beams", *Adv. Mater. Res., Int. J.*, **7**(2), 83-103. https://doi.org/10.12989/amr.2018.7.2.083

Abderezak, R., Daouadji, T.H., Rabia, B. and Belkacem, A. (2018b), "Nonlinear analysis of damaged RC beams strengthened with glass fiber reinforced polymer plate under symmetric loads", *Earthq. Struct., Int. J.*, **15**(2), 113-122. https://doi.org/10.12989/eas.2018.15.2.113

Al-Mahaidi, R. and Kalfat, R. (2011), "Investigation into CFRP laminate anchorage systems utilising bi-directional fabric wrap", *Compos. Struct.*, **93**(4), 1265-1274. https://doi.org/10.1016/j.compstruct.2010.10.012

Aslam, M., Shafigh, P., Jumaat, M.Z. and Shah, S.N.R. (2015), "Strengthening of RC beams using prestressed fiber reinforced polymers – A review", *Constr. Build. Mater.*, **82**, 235-256. https://doi.org/10.1016/j.conbuildmat.2015.02.051

Attari, N., Amziane, S. and Chemrouk, M. (2012), "Flexural strengthening of concrete beams using CFRP, GFRP and hybrid FRP sheets", *Constr. Build. Mater.*, **37**, 746-757. https://doi.org/10.1016/j.conbuildmat.2012.07.052

Belkacem, A., Tahar, H.D., Abderrezak, R., Amine, B.M., Mohamed, Z. and Boussad, A. (2018), "Mechanical buckling analysis of hybrid laminated composite plates under different boundary conditions", *Struct. Eng. Mech., Int. J.*, **66**(6), 761-769. https://doi.org/10.12989/sem.2018.66.6.761

Benhenni, M.A., Daouadji, T.H., Abbes, B., Adim, B., Li, Y. and Abbes, F. (2018), "Dynamic analysis for anti-symmetric cross-ply and angle-ply laminates for simply supported thick hybrid rectangular plates", *Adv. Mater. Res., Int. J.*, **7**(2), 119-136. https://doi.org/10.12989/amr.2018.7.2.119

Benhenni, M.A., Adim, B., Daouadji, T.H., Abbès, B., Abbès, F., Li, Y. and Bouzidane, A. (2019a), "A comparison of closed form and finite element solutions for the free vibration of hybrid cross ply laminated plates", *Mech. Compos. Mater.*, **55**(2), 181. https://doi.org/10.1007/s11029-019-09803-2

Benhenni, M.A., Daouadji, T.H., Abbes, B., Abbes, F., Li, Y. and Adim, B. (2019b), "Numerical analysis for free vibration of hybrid laminated composite plates for different boundary conditions", *Struct. Eng. Mech., Int. J.*, **70**(5), 535-549. https://doi.org/10.12989/sem.2019.70.5.535

Bensattalah, T., Zidour, M. and Daouadji, T.H. (2018), "Analytical analysis for the forced vibration of CNT surrounding elastic medium including thermal effect using nonlocal Euler-Bernoulli theory", *Adv. Mater. Res., Int. J.*, **7**(3), 163-174. https://doi.org/10.12989/amr.2018.7.3.163

Bensattalah, T., Zidour, M. and Daouadji, T.H. (2019), "A new nonlocal beam model for free vibration analysis of chiral single-walled carbon nanotubes", *Compos. Mater. Eng., Int. J.*, **1**(1), 21-31. https://doi.org/10.12989/cme.2019.1.1.021

Bouakaz, K., Daouadji, T.H., Meftah, S.A., Ameur, M., Tounsi, A. and Bedia, E.A. (2014), "A Numerical analysis of steel beams strengthened with composite materials", *Mech. Compos. Mater.*, **50**(4), 685-696. https://doi.org/10.1007/s11029-014-9435-x

Chedad, A., Daouadji, T.H., Abderezak, R., Belkacem, A., Abbes, B., Rabia, B. and Abbes, F. (2018), "A high-order closed-form solution for interfacial stresses in externally sandwich FGM plated RC beams", *Adv. Mater. Res., Int. J.*, **6**(4), 317-328. https://doi.org/10.12989/amr.2017.6.4.317

Daouadji, T.H. (2013), "Analytical analysis of the interfacial stress in damaged reinforced concrete beams strengthened by bonded composite plates", *Strength Mater.*, **45**(5), 587-597. https://doi.org/10.1007/s11223-013-9496-4

Daouadji, T.H. (2017), "Analytical and numerical modeling of interfacial stresses in beams bonded with a thin plate", *Adv. Computat. Des., Int. J.*, **2**(1), 57-69. https://doi.org/10.12989/acd.2017.2.1.057

Daouadji, T.H. and Tounsi, A. (2012), "Analyse des contraintes d'interface dans les poutres en béton armé renforcées par collage des stratifiées composites", Revue de génie industriel N° 8, 3-12.
Daouadji, T.H., Benferhat, R. and Adim, B. (2016), "Bending analysis of an imperfect advanced composite plates resting on the elastic foundations", *Coupl. Syst. Mech., Int. J.*, **5**(3), 269-285. https://doi.org/10.12989/csm.2016.5.3.269
Hadj, B., Rabia, B. and Daouadji, T.H. (2019), "Influence of the distribution shape of porosity on the bending FGM new plate model resting on elastic foundations", *Struct. Eng. Mech., Int. J.*, **72**(1), 823-832. https://doi.org/10.12989/sem.2019.72.1.061
Hassaine Daouadji, T., Benyoucef, S., Tounsi, A., Benrahou, K.H. and Adda Bedia, E.A. (2008), "Interfacial stress concentrations in FRP-damaged RC hybrid beams", *Compos. Interf.*, **15**(4), 425-440. https://doi.org/10.1163/156855408784514702
Hassaine Daouadji, T., Rabahi, A., Abbes, B. and Adim, B. (2016), "Theoretical and finite element studies of interfacial stresses in reinforced concrete beams strengthened by externally FRP laminates plate", *J. Adhes. Sci. Technol.*, **30**(12), 1253-1280. https://doi.org/10.1080/01694243.2016.1140703
Hoque, N. and Jumaat, M.Z. (2018), "Debonding failure analysis of prestressed FRP strengthened RC beams", *Struct. Eng. Mech., Int. J.*, **66**(4), 543-555. https://doi.org/10.12989/sem.2018.66.4.543
Li, J., Wang, Y., Deng, J. and Jia, Y. (2018), "Experimental study on the flexural behaviour of notched steel beams strengthened by prestressed CFRP plate with an end plate anchorage system", *Eng. Struct.*, **171**, 29-39. https://doi.org/10.1016/j.engstruct.2018.05.042
Maalej, M. and Leong, K.S. (2005), "Effect of beam size and FRP thickness on interfacial shear stress concentration and failure mode of FRP-strengthened beams", *Compos. Sci. Technol.*, **65**(7), 1148-1158. https://doi.org/10.1016/j.compscitech.2004.11.010
Mazars, J. and Pijaudier-Cabot, G. (1996), "From damage to fracture mechanics and conversely: A combined approach", *Int. J. Solids Struct.*, **33**(20), 3327-3342. https://doi.org/10.1016/0020-7683(96)00015-7
Meier, U. (1995), "Strengthening of structures using carbon fibre/epoxy composites", *Constr. Build. Mater.*, **9**(6), 341-351. https://doi.org/10.1016/0950-0618(95)00071-2
Meier, U. (2000), "Composite materials in bridge repair", *Applied Composite Materials*, **7**(2), 75-94. https://doi.org/10.1023/A:1008919824535
Mostofinejad, D. and Shameli, S.M. (2013), "Externally bonded reinforcement in grooves (EBRIG) technique to postpone debonding of FRP sheets in strengthened concrete beams", *Constr. Build. Mater.*, **38**, 751-758. https://doi.org/10.1016/j.conbuildmat.2012.09.030
Oudah, F. and El-Hacha, R. (2013), "Analytical fatigue prediction model of RC beams strengthened in flexure using prestressed FRP reinforcement", *Eng. Struct.*, **46**, 173-183. https://doi.org/10.1016/j.engstruct.2012.07.020
Rabia, B., Abderezak, R., Daouadji, T.H., Abbes, B., Belkacem, A. and Abbes, F. (2018), "Analytical analysis of the interfacial shear stress in RC beams strengthened with prestressed exponentially-varying properties plate", *Adv. Mater. Res., Int. J.*, **7**(1), 29-44. https://doi.org/10.12989/amr.2018.7.1.029
Rabia, B., Daouadji, T.H. and Abderezak, R. (2019a), "Effect of porosity in interfacial stress analysis of perfect FGM beams reinforced with a porous functionally graded materials plate", *Struct. Eng. Mech., Int. J.*, **72**(3), 293-304. https://doi.org/10.12989/sem.2019.72.3.293
Rabia, B., Daouadji, T.H. and Abderezak, R. (2019b), "Effect of distribution shape of the porosity on the interfacial stresses of the FGM beam strengthened with FRP plate", *Earthq. Struct., Int. J.*, **16**(5), 601-609. https://doi.org/10.12989/eas.2019.16.5.601
Raithby, K.D. (1982), "Strengthening of concrete bridge decks with epoxy-bonded steel plates", *Int. J. Adhes. Adhes.*, **2**(2), 115-118. https://doi.org/10.1016/0143-7496(82)90124-5
Roberts, T.M. (1989), "Approximate analysis of shear and normal stress concentrations in the adhesive layer of plated RC beams", *Struct. Engineer*, **67**(12), 229-233.
Saribiyik, A. and Caglar, N. (2016), "Flexural strengthening of RC beams with low-strength concrete using GFRP and CFRP", *Struct. Eng. Mech., Int. J.*, **58**(5), 825-845. https://doi.org/10.12989/sem.2016.58.5.825

Shen, H.-S., Chen, Y. and Su, W.-L. (2004), "Bending and vibration characteristics of damaged RC slabs strengthened with externally bonded CFRP sheets", *Compos. Struct.*, **63**(2), 231-242. https://doi.org/10.1016/S0263-8223(03)00170-3

Smith, S.T. and Teng, J.G. (2001), "Interfacial stresses in plated beams", *Eng. Struct.*, **23**(7), 857-871. https://doi.org/10.1016/S0141-0296(00)00090-0

Tahar, H.D., Boussad, A., Abderezak, R., Rabia, B., Fazilay, A. and Belkacem, A. (2019), "Flexural behaviour of steel beams reinforced by carbon fibre reinforced polymer: Experimental and numerical study", *Struct. Eng. Mech., Int. J.*, **72**(4), 409-419. https://doi.org/10.12989/sem.2019.72.4.409

Teng, J.G., Zhang, J.W. and Smith, S.T. (2002), "Interfacial stresses in reinforced concrete beams bonded with a soffit plate: a finite element study", *Constr. Build. Mater.*, **16**(1), 1-14. https://doi.org/10.1016/S0950-0618(01)00029-0

Tounsi, A. and Amara, K. (2005), "Stiffness degradation in hygrothermal aged cross-ply laminate with transverse cracks", *AIAA Journal*, **43**(8), 1836-1843. https://doi.org/10.2514/1.3925

Tounsi, A., Hassaine Daouadji, T., Benyoucef, S. and Adda Bedia, E.A. (2009), "Interfacial stresses in FRP-plated RC beams: Effect of adherend shear deformations", *Int. J. Adhes. Adhes.*, **29**(4), 343-351. https://doi.org/10.1016/j.ijadhadh.2008.06.008

Toutanji, H., Ueno, S. and Vuddandam, R. (2013), "Prediction of the interfacial shear stress of externally bonded FRP to concrete substrate using critical stress state criterion", *Compos. Struct.*, **95**, 375-380. https://doi.org/10.1016/j.compstruct.2012.08.040

Wantanasiri, P. and Lenwari, A. (2015), "Intermediate crack-induced debonding analysis for RC beams strengthened with FRP plates", *Struct. Eng. Mech., Int. J.*, **56**(3), 473-490. https://doi.org/10.12989/sem.2015.56.3.473

Wu, Q., Xiao, S. and Iwashita, K. (2018), "Experimental study on the interfacial shear stress of RC beams strengthened with prestressed BFRP rod", *Results Phys.*, **10**, 427-433. https://doi.org/10.1016/j.rinp.2018.06.007

Zhou, A., Qin, R., Feo, L., Penna, R. and Lau, D. (2017), "Investigation on interfacial defect criticality of FRP-bonded concrete beams", *Compos. Part B: Eng.*, **113**, 80-90. https://doi.org/10.1016/j.compositesb.2016.12.055

CH